# DERIVATION OF UNSTEADY AERODYNAMIC MODELS FROM WIND TUNNEL MULTI-AXIS TEST RIGS

**Mark Lowenberg, Hilton Kyle**
**University of Bristol, UK**

**Keywords**: *Unsteady Aerodynamic Modelling, Dynamic Test Rigs*

## Abstract

*The execution of certain types of manoeuvres in fighter aircraft, missiles and future uninhabited air vehicles, such as in post-stall manoeuvring, results in aerodynamic loads with significant time–dependent flows. Existing mathematical models do not account for these unsteady aerodynamic loads, and when used for design and analysis encompassing time-dependent regimes, can result in unacceptable errors.*

*Improved model formulations can represent aerodynamic loads associated with manoeuvring aircraft but require enhanced experimental apparatus. New dynamic test rigs must facilitate the acquisition of load and/or motion data under large-amplitude motions at representative rates, as well as being capable of evaluating model support influences, multiple-axis coupled motions and the effects of moving surfaces on the model.*

*This paper discusses the need for improved model formulations and, consequently, the need for alternative dynamic testing facilities. We then describe the project being undertaken at the University of Bristol on development of a pilot rig for multi-axis large-amplitude dynamic wind tunnel testing. Experimental results and computational modelling of the rig dynamics are also included. A model is derived to represent longitudinal limit cycle behaviour.*



## 1 Unsteady aerodynamic modelling

The traditional experimental basis for developing a mathematical model that describes the aerodynamic loads on an aircraft is the execution of static and dynamic wind tunnel tests. The latter usually comprise small-amplitude oscillatory tests and rotary balance techniques, allowing the determination of damping and $\dot{\alpha}$ and $\dot{\beta}$ derivatives. Non-linearity is accounted for simply by tabulating the derivatives as functions of, for example, incidence and Mach number; rate dependence is represented in terms of frequency.

When aircraft perform large-amplitude manoeuvres or undergo rapid oscillatory autorotations (spins), phenomena such as flow separation, vortex bursting and attachment may play important roles in the production of aerodynamic loads. The result is that aerodynamic coefficients vary with motion variables in a non-linear manner and the times associated with various flow adjustments mean that the coefficients depend on the motion history.

This time-dependency creates a problem for flight mechanics modelling. The traditional stability derivative formulation typically allows for rate of change of motion but does not admit time lags, hysteresis, etc. This approach has been remarkably succesful for most types of fixed-wing air vehicle over many decades. However, it is well recognized that time

dependence in the aerodynamic loading is not accounted for via such models, and that this poses problems for modelling of highly-manoeuvrable aircraft, low-speed flight in gusts, etc. Even for more benign flight regimes, the attempt to capture time dependence via tabulating derivatives against frequency produces erroneous models [1].

Various suggestions for improved modelling have been made, mainly based on indicial responses or state-space/characteristic time constant models [e.g.1,2,3,4,5,6]. These methods attempt to account explicitly for the transient effects on loading by relating them to motion characteristics.

To illustrate the need for proper unsteady models – and consequently for suitable test rigs – we consider representing the rolling moment for a 65° delta-wing (from experimental data), using two methods:

- a formulation from [5] that uses linear indicial responses to incorporate time dependence, and
- a traditional stability derivative representation.

The indicial response (IR) model consists of a potential flow and a vorticial contribution, and may be written as:

$$\left.\begin{aligned} \mathrm{C}\ell = C\ell^{v}_{s}(0) + C\ell^{p}_{s}(\phi(t)) + \\ C\ell^{v}_{s_{lag}}(t) + \mathrm{C}\ell^{p}_{\dot{\phi}}\dot{\phi}(t) + \mathrm{C}\ell^{v}_{\dot{\phi}_{lag}}(t) \end{aligned}\right\} \quad (1)$$

where:

$C\ell^{v}_{s}(0)$ = initial static equilibrium condition of the vorticial rolling moment

$C\ell^{p}_{s}(\phi(t))$ = static potential contribution

$C\ell^{v}_{s_{lag}}(t)$ = lag of the static vorticial contribution

$\mathrm{C}\ell^{p}_{\dot{\phi}}$ = potential roll-damping derivative

$\mathrm{C}\ell^{v}_{\dot{\phi}_{lag}}(t)$ = lag of the dynamic vorticial contribution

The static and dynamic potential terms are determined using a panel method, and the static and dynamic vorticial contributions – which incorporate the time lags – are defined in transfer function format (using experimental data).

The stability derivative (SD) formulation is simply:

$$\mathrm{C}\ell = \mathrm{C}\ell_{\phi}.\phi + \mathrm{C}\ell_{\dot{\phi}}.\dot{\phi} \quad (2)$$

However, to isolate the discrepancies due to time dependencies from the effects of non-linearities, the static part of equation (2) was taken as the static part of equation (1):

$$\mathrm{C}\ell_{\phi}.\phi \equiv C\ell^{v}_{s}(0) + C\ell^{p}_{s}(\phi(t)) + C\ell^{v}_{s}(\phi(t)). \quad (3)$$

The term $C\ell_{\dot{\phi}}$ was obtained by evaluating the out-of-phase components of the $C_{\ell}$ data for each of the three frequencies for which experimental data exist [1,7].

Figure 1 shows a comparison between the IR and SD models for sinusoidal rolling input motion of ±3° amplitude and 7.7Hz frequency. It is clear that there is a difference in both shape and maximum amplitude. The shape of the SD model output arises from an asymmetric static moment variation; the difference relative to the IR model is due to the inability of the SD model to account for transient loads.

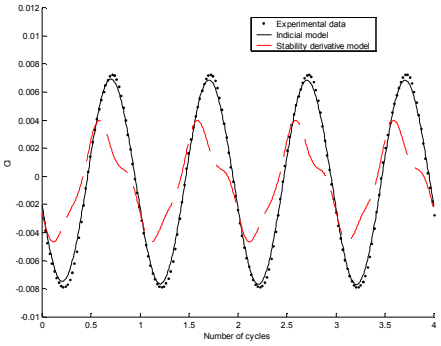

Figure 1: Time history comparison of IR and SD models ($\phi$ input: ±3°, 7.7Hz).

Although the above results are for a simple one degree-of-freedom (1-DOF) system oscillating at small amplitude, they demonstrate some of the issues in aerodynamic modelling and experimental requirements. Multi-DOF aircraft motions are substantially more complex since longitudinal and lateral-directional time dependancies will usually be coupled [4].

An obvious solution is to deploy oscillatory rigs at larger amplitudes, and to combine oscillatory motion with coning. There are, however, difficulties with such approaches, such as the power requirement to achieve high-rate motions and demands on support structure (rigid stings are usually used, increasing interference effects). Furthermore, it is difficult with these 'inexorable drive' rigs to achieve arbitrary multi-degree-of-freedom motions; and the aerodynamic influences of control surface movements during manoeuvres are not captured.

In order to generate data suitable for modelling unsteady aerodynamic loads during manoeuvres in which significant control surface movement may be present, a dynamic wind tunnel rig must provide:

(i) multiple degree of freedom, to supply data for coupled motions;
(ii) large amplitude arbitrary motions;
(iii) high motion rates;
(iv) vehicle configuration changes during manoeuvres (control surface movements);
(v) minimal support interference;
(vi) low operating power requirements;
(vii) tests on inherently unstable aircraft models if necessary.

## 2 Pendulum support rig (PSR)

A novel rig configuration that meets the above criteria is the 'pendulum rig' [4], Figure 2. 2-DOF and 5-DOF pilot rigs are being developed for the University of Bristol open-jet wind tunnel.

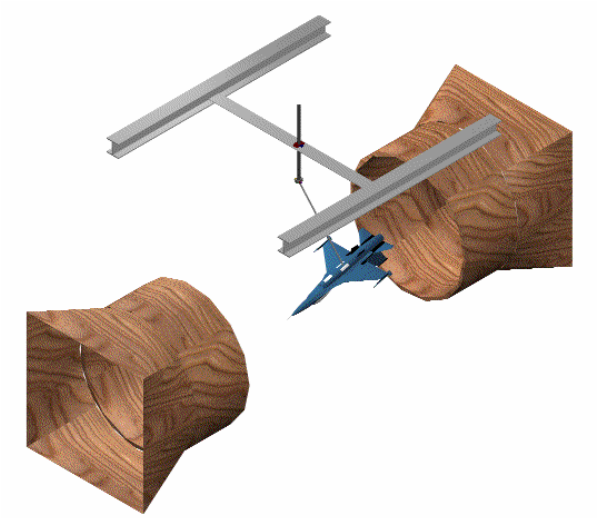

Figure 2: Schematic of 5-DOF pendulum support rig in open-jet wind tunnel

The 5-DOF rig design consists of a movable and remotely controlled aircraft model suspended in a wind tunnel on a pendulum strut. The aircraft has three angular and two translational degrees-of-freedom, and may be suspended in an upright or inverted position. The model is essentially 'flown' in the tunnel, with control and data logging effected via a PC. A gimbal joint connects the aircraft to the pendulum strut, which is attached to the rig support system via a second gimbal. Large amplitudes are possible (40° pitch range); arbitrary combinations of pitch and heave can be achieved (within the constraints of the pendulum kinematics); and the loads on the strut are low, reducing sting interference effects.

The rig is intended primarily as a pilot project of low cost and simple construction, and is aimed at justifying the viability of the pendulum strut approach. Design considerations have included motion amplitudes and rates, mass and inertia scaling, control and data acquisition limitations, and friction and interference effects.

It was decided to implement a 2-DOF version of the pendulum rig before progressing to the more complex 5-DOF system. This contains the two

longitudinal degrees of freedom, pitch and heave (via swing of the pendulum in the longitudinal sense), and is shown with the Hawk model installed in Figure 3. A picture of the assembled Hawk model is shown in Figure 4, and Figure 5 shows the model separated into its various components. The model is not an exact replica of the full-sized Hawk, as it is not intended to achieve full dynamic similarity due to the limitations of the wind tunnels at the University.

Figure 3: Pendulum rig layout in open-jet tunnel.

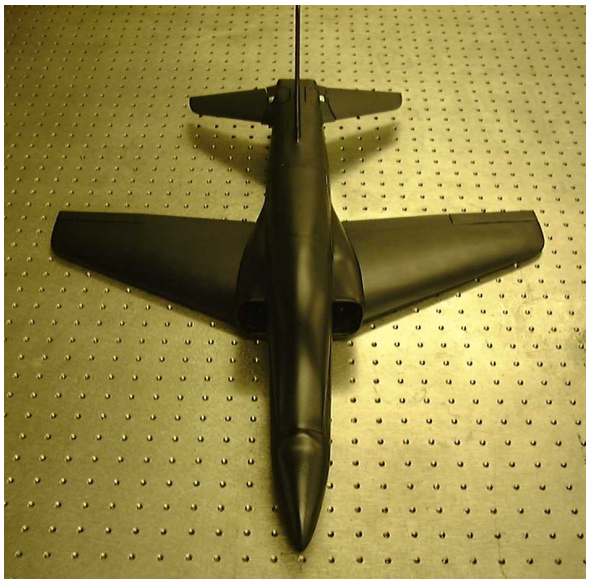

Figure 4: Assembled Hawk model

Figure 5: Disassembled Hawk model, showing various components

Both the 2-DOF and later the 5-DOF rigs will be used for:

a) physical 'simulation' of aircraft model dynamics at high angles of attack.
b) development of non-linear unsteady aerodynamic models using parameter identification. In particular, models such as that in equation (1) will be explored and ultimately extended to multiple degrees-of-freedom.
c) assessment of different control laws.
d) investigation of flight control laws of aircraft with redundant control surfaces.

The aircraft model chosen for early work on the 2-DOF system is a $1/16^{th}$-scale BAe Hawk, with a wing span of 600 mm and approximate weight of 1.2 kg. It is based on drawings for a $1/8^{th}$-scale radio-controlled model but with significant differences:

- higher-strength wooden structure, with fibreglassed outer surface coatings;

- fuselage-mounted servo drives for the control surfaces, with ailerons connected via torque tubes while the elevator and rudder are driven directly (note that the rudder and ailerons are not actuated in 2-DOF tests);
- separate left- and right-hand elevator servo's (to allow differential tailplane angles, aimed primarily at reconfigurable control tasks);
- a removable ducted fan powerplant;
- and the obvious modifications to accommodate the gimbal attachment (currently the 2-DOF system but designed for later use with a 5-DOF attachment), in which the strut can enter from the underside or topside of the model.

The possibility of operating the system with the ducted fan installed permits thrust effects to be incorporated within measurements and evaluations. It will not, however, produce sufficient thrust to permit full 6-DOF suspension.

## 2.1 Load measurement

For the purposes of unsteady aerodynamic data gathering, it is desirable to include meaurement of the aerodynamic lift and drag reaction: this offers the prospect of aiding parameter estimation and provides information on the lag between the load and the response. Two flexures have been designed for this purpose: a 'binocular' configuration strain gauge balance (fitted midway along the strut) and a 'ring' balance (virtually integral with the model gimbal, to minimise exposure to strut bending). Whilst designed to measure tension in the strut, there is also coupling with the bending loads that arise in the 2-DOF rig. The flexure geometries were refined using finite element analysis (see Figures 6 and 7), and the top of the strut is gauged to measure bending loads, thus permitting a full calibration to be conducted. Figure 8 shows an output from the binocular transducer, indicating a lag between the model motion and lift produced.

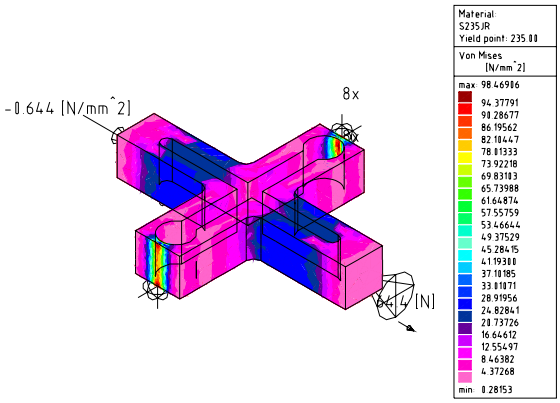


Figure 6: FEM analysis of 'binocular' type transducer

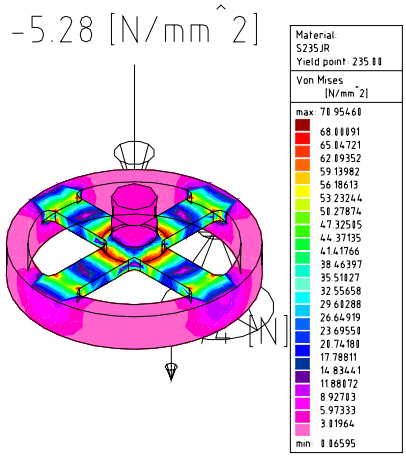


Figure 7: FEM analysis of 'ring' type transducer

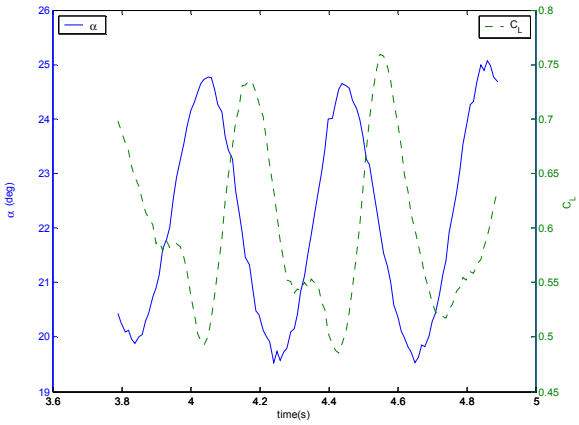


Figure 8: Hawk model unconstrained stabilator sinusoidal response, $\alpha_{nom} \approx 22.5°$ (solid line=$\alpha$, dashed line=$C_L$).

## 2.2 Real time control

The key to physical simulation via rigs such as this is effective real-time control. This has been achieved using a DSpace system, operating in

the MATLAB/Simulink environment. A brief specification of the system is:

- 16 channel ADC (16 bit precision, 4µs conversion time)
- 4 channel ADC (12 bit precision, 800ns conversion time)
- 8 channel DAC (14 bit precision, 5µs settling time)
- 6 position encoder inputs
- 5 Pulse Width Modulated (PWM) outputs
- 32 bits of digital I/O.

## 3 Stability issues

Work carried out in 1994 at the Central Aerohydrodynamic Institute (TsAGI) in Russia suggested that the PSR with a stable aircraft model mounted inverted would be stable [4]. In the upright-mounted system, the instability led to large amplitude stable pitch oscillations (limit cycles). It was proposed that the resulting plunging motions could in principle be used to separately determine rotary and translational aerodynamic derivatives. In other words, instability of the model-pendulum combination need not necessarily preclude testing in such regions.

As part of the rig and aerodynamic model development, a numerical analysis of the combined dynamical system behaviour is undertaken. In the case of the 2-DOF rig, the PSR dynamics is described by a 4$^{th}$ order set of equations. Bifurcation analysis is implemented (using the software code AUTO) to determine the steady state solutions (equilibria and periodic orbits) and their stability as parameters (e.g. tailplane deflection, wind speed) vary. This allows a close check to be made on any regions of instability and the nature of such behaviour. However, the equations include aerodynamic forces and moments, so that the process is iterative and becomes more accurate as the aerodynamic model develops.

Figure 9 shows a sample bifurcation diagram for the 2-DOF PSR (not using Hawk aerodynamic data), revealing regions where the equilibria are unstable. Figure 10 is a time history showing a limit cycle solution that is of interest because the strut angle is dominant whilst the 'aircraft' mode (pitch angle) exhibits negligible oscillation.

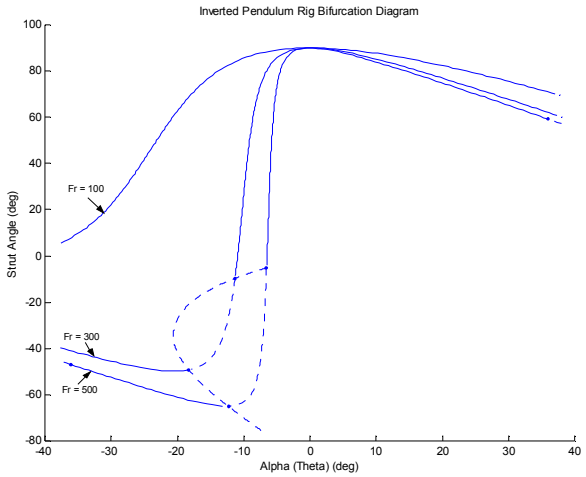


Figure 9: Bifurcation diagram showing paths of equilibria for three Froude no's and locus of Hopf bifurcation points; 2-DOF PSR, hypothetical aircraft model.

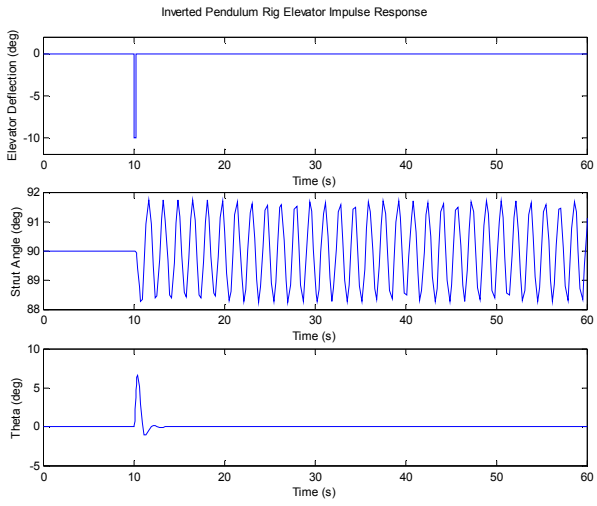


Figure 10: Time history showing oscillatory response in strut angle; 2-DOF PSR, hypothetical aircraft model.

### 3.1 Limit cycle behaviour

Initial 2-DOF testing reavealed the presence of two regions of limit cycle bahvaiour, at approximately $\alpha$ = 5° and 22°. Fig 11 shows these two regions, and was obtained by quasi-statically varying tailplane deflection, and holding the incidence angle steady for a fixed

period of time. The graph was constructed by plotting those values at which pitch rate, $q$, was zero. However, due to experimental noise and wind tunnel turbulence, points that had a pitch rate of less than |2|° were plotted.

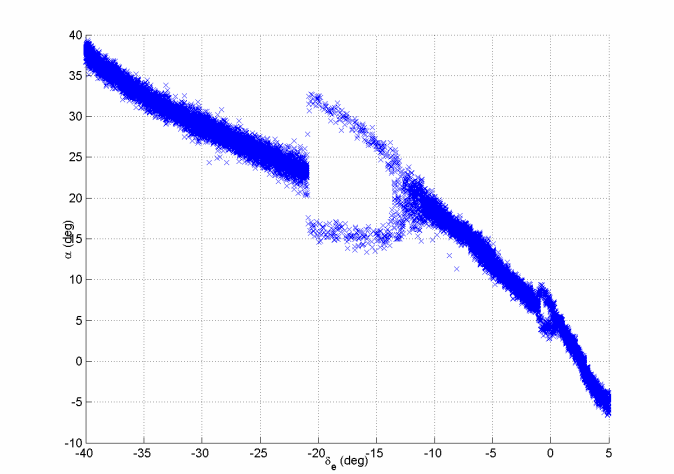


Figure 11: Experimental bifurcation diagram for 2-DOF PSR

Static pitching moment tests performed on the model did not show any regions of static instability in the limit cycle region, with $C_{m_\alpha}$ varying from –1.0 to –1.8 rad$^{-1}$.

To develop a mathematical model able to predict the limit cycle behaviour, the pitching moment acting on the aircraft is first calculated, for motion in 1-DOF only. It is assumed that the pitch acceleration $\ddot{\alpha}$ is proportional to the pitching moment, $C_m$:

$$\frac{1}{2}\rho V^2 S\bar{c}C_m = I\ddot{\alpha} \qquad (4)$$

where $I$ = model pitching inertia.

The pitch angle data is first passed through a filter with a 30rad/s bandwith, in both the forward and reverse directions to eliminate any time delay occuring due to the filtering process. The acceleration (second derivative) of the data is then calculated, and hence $C_m$ is determined as a function of $\alpha$.

Due to wind tunnel noise, the amplitude and frequency of the limit cycle varied slightly, and hence a plot of $C_m$ vs $\alpha$ showed slightly inconsistent behaviour. Most inexorable drive rigs impart motion through a fixed amplitude, which does not vary for each cycle of the motion. Due to the nature of the rig, the maximum amplitude of each cycle shows slight variation, and hence being able to formulate motion and aerodynamic variables as a function of pitch angle is slightly problematic.

To eliminate this, the average frequency and amplitude for a particular dataset was calculated, and all data was normalised with respect to these two variables. This resulted in Figure 3, a plot of $C_m$ *vs* $\alpha$.

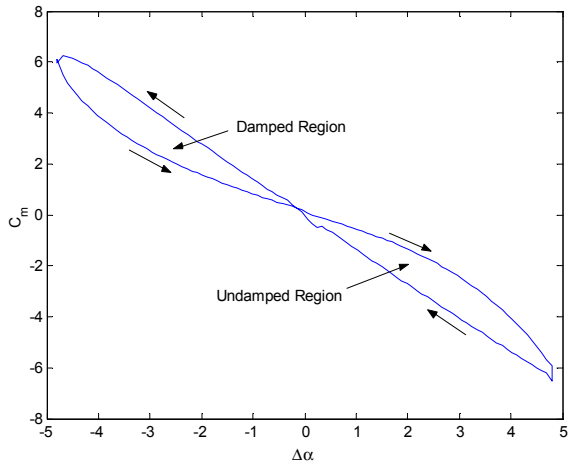


Figure 12: Cross-plot of $C_m$ *vs* $\Delta\alpha$, $\alpha_{\text{nom}} \approx 20^\circ$.

Fig 11 shows two distinct regions, one damped (clockwise motion) and undamped (anti-clockwise). This is somewhat unusual for limit cycle behaviour, where limit cycle motion is usually governed by motion from one damped region to another, with a negatively damped region in-between to drive the continuous motion. The amplitude of such motion is primarily governed by the size of this negatively damped region, as well as the value of the damping in both stable regions. The limit cycle shown by the Hawk model does not show any such middle region of negative damping to drive the motion, and hence a standard model will not predict this behaviour.

To represent the motion , a model structure of the following form was proposed (in transfer function format):

$$\ddot{\alpha} = -\frac{c}{I}\dot{\alpha} - \frac{k}{I}\alpha \qquad (5)$$

$$\text{where} \quad c = -\frac{1}{2}\rho V S \bar{c}^2 C_{m_q}\left(\frac{1}{1+\tau_c s}\right) \qquad (6)$$

$$C_{m_q} = A_c(\alpha - c_{offset})^3 \qquad (7)$$

and

$$k = \frac{1}{2}\rho V^2 S \bar{c} C_{m_\alpha}(\alpha - k_{offset})\left(\frac{1}{1+\tau_k s}\right) \qquad (8)$$

The above equations correspond to that of a spring-mass damper system.

Parameter estimation resulted in the following values:

| | |
|---|---|
| $C_{m_\alpha}$ (rad$^{-1}$) | –1.24 |
| $A_c$ | –0.00155 |
| $\tau_c$ | 0.04 |
| $\tau_k$ | 0.004 |
| $k_{offset}$ | 0.8 |
| $c_{offset}$ | 0.8 |

It was assumed that $C_{m_\alpha}$ was not a function of $\alpha$, and the estimated value of –1.24 rad$^{-1}$ compares favourably to that estimated from static wind tunnel testing. The time constants were added so as to ensure that the model motion was not dependant on initial conditions, and that the amplitude of the pitch motion converged to the steady state limit cycle.

Figure 12 shows the model prediction $C_m$ compared to the experimental data, as a function of $\alpha$. Figure 13 shows the model fit for a limit cycle at a mean pitch angle of $\alpha$ = 20° and elevator deflection of –13°.

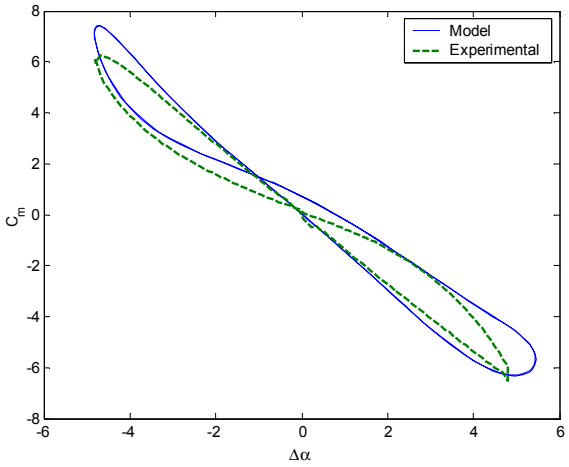


Figure 13: $C_m$ vs $\alpha$ of model and experimental data for limit cycle oscillations at $\alpha_{\text{nom}} \approx 20^\circ$

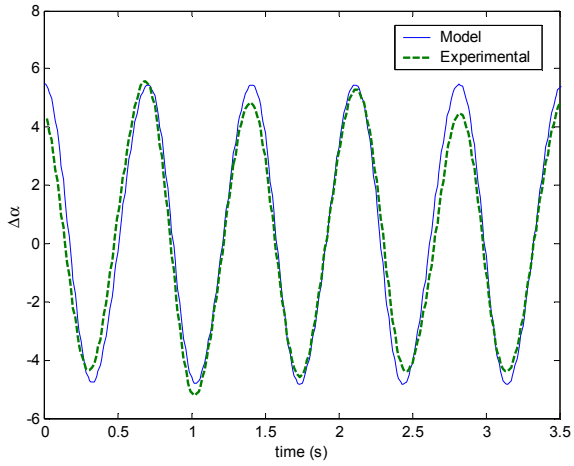


Figure 14: $\alpha$ vs time of model simulation and experimental data for limit cycle oscillations at $\alpha_{\text{nom}} \approx 20^\circ$

## 4 Future 5-DOF PSR

Once the PSR/active control concept has been proved on the 2-DOF system, it is planned to create a 5-DOF version. Where possible, the two will use common elements, so that a model can be made to operate with either rig.

The 5-DOF rig design endows the model with three angular and two translational degrees-of-freedom, and may be suspended in an upright or inverted position. While the 2-DOF apparatus

has a single-DOF pivot between the model and strut, in the 5-DOF rig this is a 3-axis gimbal joint. The pendulum is attached above or below the working section to a rigid rig support system via a 2-DOF gimbal. A sketch of the 5-DOF PSR configuration in an open-section wind tunnel is shown in Figure 2. Clearly, both the control and the modelling challenge are significantly greater for the 5-DOF system than for the 2-DOF case.

## 5 Conclusions

Some of the challenges in mathematical modelling of time-dependant flow phenomena have been illustrated. These have an impact on experimental facilities used to generate modelling data, in this case rigid-body dynamic wind tunnel rigs. To facilitate unsteady aerodynamic measurements, large-amplitude multiple-DOF motions are necessary. The pendulum rig apparatus under development at the University of Bristol was then discussed, and the existing 2-DOF rig and aircraft model described. The limit cycle behaviour of the rig was described, as well as a mathematical model that predicts this non-linear phenomenon.

## Acknowledgements

The authors are grateful for the funding received from QinetiQ Bedford towards development of the PSR rig . Thanks is due to Dr D. Greenwell (previously of QinetiQ Bedford) and Prof. M Goman at de Montford University for proposing the pendulum test rig development, and to Dr J. Myatt of the Air Force Research Laboratory, WPAFB, USA for supplying the 65° delta wing data. The work of Paul Davison in producing Figures 9-11 is also appreciated.

## References

[1] GREENWELL, D.I. *Modelling of frequency effects on aerodynamic derivatives obtained from small-amplitude oscillatory testing*, Report no. DERA/AS/HWA/ TR97006/1, Defence Evaluation & Research Agency, UK, Feb. 1997.

[2] GOMAN, M.G. and KHRABROV, A. State-space representation of aerodynamic characteristics of an aircraft at high angles of attack, *J. Aircraft*, 1994, 31(5), pp 1109-1115.

[3] GOMAN, M.G., GREENWELL, D.I. and KHRABROV, A.N. The Characteristic Time Constant Approach for Mathematical Modelling of High Angle of Attack Aerodynamics, *Proceedings of ICAS Congress*, 2000.

[4] GOMAN, M. *Mathematical modelling of high angles of attack aerodynamics for solving flight dynamics problems*, Research Monograph 13, School of Computing Sciences, De Montfort University, 1997.

[5] MYATT, H.J. *Modelling the Rolling Moment on the 65-degree Delta Wing for Rolling Motions at High Angle of Attack*, PhD thesis, Stanford University, 1997.

[6] TOBAK, M. and SCHIFF, L.B. Aerodynamic mathematical modelling – basic concepts, *AGARD Lecture Series on Dynamic Stability Parameters*, AGARD-LS-114, NATO, 1981.

[7] Hanff, E.S. Direct forced-oscillation techniques for the determination of stability derivatives in wind tunnels, lecture 4 in *AGARD Lecture Series on Dynamic Stability Parameters*, AGARD-LS-114, NATO, Mar. 1981.